Pore formation and rupture in fluid bilayers

Roland R. Netz and M. Schick
Department of Physics, Box 351560, University of Washington, Seattle, Washington 98195-1560
(Received 14 November 1995)

Structure and stability of fluid bilayers under stress are examined by modeling lipid as diblock copolymer and solvent as homopolymer. The model is solved using self-consistent field theory, and equilibrium phases are determined. We find that on increasing the stress applied to the bilayer, one of two scenarios occurs depending upon the architecture of the lipid. Either the bilayer ruptures, or pores form within it and condense into a regular array. In the former case, the fractional increase in area from its unstressed value is found to be approximately 2% at rupture, in satisfactory agreement with experiment. In the latter, the pores appear and disappear reversibly with the stress, in accord with experiment. We find the pores to be slightly hydrophobic.

PACS number(s): 83.70.Hq, 87.22.Bt, 36.20.−r

I. INTRODUCTION

Bilayer membranes are interesting for many reasons, among which are the facts that they serve as simple models of biological membranes, and promise a wide range of applications in industry and medicine [1–5]. Of vital importance to the functioning of living cells and to many applications is the stability of membranes against external perturbations [6]. Consequently, much attention has been paid to the mechanical properties of membranes [7–12].

In a series of experiments [13,14], unilamellar vesicles were subjected to lateral stresses to the point of rupture. One of the many interesting results of these experiments is that the membrane cannot support much strain; the relative increase in area of the membrane at the point of rupture is only about 2–3%. This was somewhat of a surprise in that a simplified model calculation yields an instability at an area increase an order of magnitude larger [15].

Interest in the mechanical properties of membranes has greatly increased with the introduction of electroporation, a process by which the application of a short, intense electric field subjects the membrane to an effective compressive stress leading to a *reversible* dielectric breakdown of the membrane due to the formation of pores [16,17]. These pores can be utilized to incorporate specific genes, proteins, or other macromolecules into a large number of isolated cells. Although clearly of great importance, the phenomenon and the underlying microscopic mechanism are as yet poorly understood. One of the important issues in the theories of electroporation is the nature of the pores, in particular whether the tails of the lipids are exposed to water in the formation of the pore, or are shielded by a rearrangement of head groups.

In this paper we investigate the response of a membrane to stress by means of a polymeric model for bilayer membranes, taking into account both internal degrees of freedom of the lipids and interactions between the lipids and the solvent molecules. The formation of small holes, or pores, and the fragmentation, or rupture, of the membrane are both obtained as *distinct equilibrium* mechanisms for permeabilization. Solvent and lipid are modeled as A homopolymer and AB diblock, respectively, and are described by the usual Edwards Hamiltonian for flexible chains. This model is solved within the self-consistent field theory as a function of the applied mechanical stress. Depending on the molecular architecture of the "lipid," compression of the membrane leads either to the formation of small, stable pores, or to rupture, i.e., to the fragmentation of the membrane into a undisturbed region and a disordered, solventlike region. The maximal relative area increase of the membrane at rupture is found to be approximately 2% for the parameters used, and is thus very close to the experimentally measured values. A catenoid lamellar phase, which represents a condensation of pores into a hexagonal array, is examined and we find that the pores thus formed are slightly hydrophobic; i.e., the interior groups of the chains are exposed to the solvent.

II. POLYMERIC MODEL FOR SWOLLEN BILAYERS

In several models of bilayer membranes, the presence of solvent is neglected, and only the statistics of the lipids confined to a slab of finite thickness are considered [18,19]. In other models, the surrounding solvent, which contains a nonzero concentration of lipid, is taken into account, but the lipids are treated as objects without internal degrees of freedom [20]. However, to encompass changes in bilayer properties due to applied stress, changes such as the appearance of pores, a model must incorporate both the internal and translational degrees of freedom of lipids and their interaction with the surrounding solvent. We construct such a model below in which diblock copolymers and homopolymers play the roles of lipid and solvent, respectively. In a wide range of the space of parameters, such as copolymer architecture and strength of interaction between membrane and solvent, the phase of lowest free energy corresponds to an array of parallel bilayers separated by solvent. The array is characterized by two length scales, the wavelength, or repeat distance, and the bilayer thickness. Both lengths vary with the concentration of solvent, which solubilizes a small fraction of copolymer. In lipid-water systems, the concentration of lipid solubilized in water is very small. Nevertheless, bilayers cannot be formed until a certain threshold of solubilized lipid, the critical micelle concentration (cmc), is attained. In principle, *isolated* bilayers can only be formed in equilibrium precisely at the cmc. At larger lipid concentrations, a lamellar phase with a finite wavelength would be expected. To this extent, experiments performed on isolated bilayers are not strictly in equilibrium. However, we expect the results of our equilibrium study of membrane stacks to be applicable to experi-

ments on isolated bilayers provided that we examine results in the limit of large lamellar separation.

To investigate the effect of stress on a lamellar phase, we consider such a phase in a system of flexible polymers. AB diblock copolymers of polymerization index N play the role of lipids, and A homopolymers of index gN play the role of water. The A segments of the copolymers with relative length f correspond to the lipid heads, and the B segments with relative length $1-f$ correspond to the tails. The formation of bilayer structures is induced by a repulsion between A and B monomers. The system is assumed to be incompressible. Each monomer occupies a volume $1/\rho_0$, therefore the system of n_C copolymers and n_H homopolymers occupies a total volume $V=(n_C+gn_H)N/\rho_0$. The volume fractions of copolymers and homopolymers are given by $\phi_C=n_C/(n_C+gn_H)$ and $\phi_H=gn_H/(n_C+gn_H)$, respectively. Each polymer is parametrized by a variable s that increases continuously along its length. For the copolymers, we choose $s=0$ at the A-monomer end, so that $s=f$ at the junction point, and $s=1$ at the other end. For the homopolymers, s varies between 0 and g. Using this parametrization, we define functions $\mathbf{r}_\alpha^C(s)$ and $\mathbf{r}_\beta^H(s)$ that specify the space curves occupied by the αth copolymer and βth homopolymer.

The partition function, which contains the incompressibility condition, is given by

$$Z=\frac{1}{n_C!n_H!}\int\prod_{\alpha=1}^{n_C}\mathscr{D}\mathbf{r}_\alpha^C P[\mathbf{r}_\alpha^C(\cdot);0,1]\int\prod_{\beta=1}^{n_H}\mathscr{D}\mathbf{r}_\beta^H \times P[\mathbf{r}_\beta^H(\cdot);0,g]\delta[1-\hat{\Phi}^A-\hat{\Phi}^B] \times\exp\left\{-\chi\rho_0\int d\mathbf{r}\hat{\Phi}^A\hat{\Phi}^B\right\}, \tag{1}$$

where the functional integrals over all copolymer and solvent polymer configurations are weighted with the Wiener measure

$$P[\mathbf{r}(\cdot);s_1,s_2]=\exp\left\{-\frac{3}{2Na^2}\int_{s_1}^{s_2}ds\left(\frac{d}{ds}\mathbf{r}(s)\right)^2\right\}. \tag{2}$$

The Kuhn length a is assumed to be the same for all monomers. The Flory-Huggins parameter χ measures the incompatibility of the A and B monomers. The dimensionless monomer densities are defined by

$$\hat{\Phi}^A(\mathbf{r},\{\mathbf{r}_\alpha^C(\cdot)\},\{\mathbf{r}_\beta^H(\cdot)\})=\frac{N}{\rho_0}\sum_{\alpha=1}^{n_C}\int_0^f ds\,\delta[\mathbf{r}-\mathbf{r}_\alpha^C(s)] +\frac{N}{\rho_0}\sum_{\beta=1}^{n_H}\int_0^g ds\,\delta[\mathbf{r}-\mathbf{r}_\beta^H(s)], \tag{3}$$

$$\hat{\Phi}^B(\mathbf{r},\{\mathbf{r}_\beta^H(\cdot)\})=\frac{N}{\rho_0}\sum_{\alpha=1}^{n_C}\int_f^1 ds\,\delta[\mathbf{r}-\mathbf{r}_\alpha^C(s)]. \tag{4}$$

Note that the $\hat{\Phi}^A$ depend explicitly on the configurations of all polymers containing A monomers, and similarly for $\hat{\Phi}^B$. It is this explicit dependence in the product $\hat{\Phi}^A\hat{\Phi}^B$ that makes Eq. (1) so intractable. To make it somewhat more amenable, one inserts a functional integral, $1=\int\mathscr{D}\Phi^A\mathscr{D}\Phi^B\delta[\Phi^A-\hat{\Phi}^A]\delta[\Phi^B-\hat{\Phi}^B]$, which permits replacement of the densities $\hat{\Phi}^A(\mathbf{r},\{\mathbf{r}_\alpha^C(\cdot)\},\{\mathbf{r}_\beta^H(\cdot)\})$ and $\hat{\Phi}^B(\mathbf{r},\{\mathbf{r}_\beta^H(\cdot)\})$, which depend upon the polymer configurations, by the functions $\Phi^A(\mathbf{r})$ and $\Phi^B(\mathbf{r})$, which do not. Inserting standard representations for the δ functionals, using the incompressibility constraint, and carrying out a Gaussian functional integral over Φ^A, one obtains

$$Z=\mathscr{N}\int\mathscr{D}w^A\mathscr{D}w^B\exp\{-F[w^A,w^B]/k_BT\}, \tag{5}$$

where $\mathscr{N}$ is a normalization constant and

$$\frac{F[w^A,w^B]}{(n_C+n_Hg)k_BT}\equiv-\frac{n_C}{n_C+gn_H}\ln\frac{\mathscr{Q}^C}{n_C}-\frac{n_H}{n_C+gn_H}\ln\frac{\mathscr{Q}^H}{n_H} +V^{-1}\int d\mathbf{r}\left\{\frac{\chi N}{4}\left[\frac{w^A(\mathbf{r})-w^B(\mathbf{r})}{\chi N}-1\right]^2 -w^B(\mathbf{r})\right\}, \tag{6}$$

where

$$\mathscr{Q}^C\equiv\int\mathscr{D}\mathbf{r}_\alpha^C P[\mathbf{r}_\alpha^C(\cdot);0,1]\exp\left\{-\int_0^f ds w^A(\mathbf{r}_\alpha^C(s)) -\int_f^1 ds w^B(\mathbf{r}_\alpha^C(s))\right\} \tag{7}$$

and

$$\mathscr{Q}^H\equiv\int\mathscr{D}\mathbf{r}_\beta^H P[\mathbf{r}_\beta^H(\cdot);0,g]\exp\left\{-\int_0^g ds w^A(\mathbf{r}_\beta^H(s))\right\} \tag{8}$$

are the partition functions of single copolymers and homopolymers subject to external potentials $w^A(\mathbf{r})$ and $w^B(\mathbf{r})$. Equation (5) expresses the partition function of the many polymer system in terms of the partition functions of single polymer systems subject to external, fluctuating, fields. The self-consistent field theory approximates this functional integral over the fields by the value of the integrand evaluated at those values of the fields, W^A, W^B, which minimize the functional $F[w^A,w^B]$. From the definition of F, it follows that these functions satisfy the self-consistent equations

$$W^A(\mathbf{r})-W^B(\mathbf{r})=\chi N(1-2\phi^A(\mathbf{r})), \tag{9}$$

and

$$\phi^A(\mathbf{r})+\phi^B(\mathbf{r})=1, \tag{10}$$

where

$$\phi^A(\mathbf{r})\equiv -\frac{n_C}{n_C+gn_H}\frac{V}{\mathcal{Q}^C}\frac{\mathcal{D}\mathcal{Q}^C}{\mathcal{D}W^A(\mathbf{r})} -\frac{n_H}{n_C+gn_H}\frac{V}{\mathcal{Q}^H}\frac{\mathcal{D}\mathcal{Q}^H}{\mathcal{D}W^A(\mathbf{r})}, \tag{11}$$

$$\phi^B(\mathbf{r})\equiv -\frac{n_C}{n_C+gn_H}\frac{V}{\mathcal{Q}^C}\frac{\mathcal{D}\mathcal{Q}^C}{\mathcal{D}W^B(\mathbf{r})}, \tag{12}$$

are the average volume fractions at $\mathbf{r}$ of monomers A and B respectively. Thus, the free energy density $\mathcal{F}$ is approximated by $F[W_A,W_B]/V$, with F given in Eq. (6). To obtain the single particle partition functions, one defines the end-segment distribution functions

$$q_C(\mathbf{r},s)\equiv\int \mathcal{D}\mathbf{r}_\alpha^C P[\mathbf{r}_\alpha^C;0,s]\delta[\mathbf{r}-\mathbf{r}_\alpha^C(s)]\exp\left\{-\int_0^s dt[\gamma(t)W^A(\mathbf{r}_\alpha^C(t))+(1-\gamma(t))W^B(\mathbf{r}_\alpha^C(t))]\right\}, \tag{13}$$

$$q_H(\mathbf{r},s)\equiv\int \mathcal{D}\mathbf{r}_\beta^H P[\mathbf{r}_\beta^H;0,s]\delta[\mathbf{r}-\mathbf{r}_\beta^H(s)]\exp\left\{-\int_0^s dt W^A(\mathbf{r}_\beta^H(t))\right\}, \tag{14}$$

from which $\mathcal{Q}^C=\int d\mathbf{r}q_C(\mathbf{r},1)$ and $\mathcal{Q}^H=\int d\mathbf{r}q_H(\mathbf{r},g)$. The step function $\gamma(t)$ is equal to 1 for $t<f$ and 0 otherwise. The distribution functions satisfy the diffusion equation

$$\frac{\partial q_C}{\partial s}=\frac{1}{6}Na^2\nabla^2 q_C-\gamma(s)W^A(\mathbf{r})q_C-[1-\gamma(s)]W^B(\mathbf{r})q_C, \tag{15}$$

$$\frac{\partial q_H}{\partial s}=\frac{1}{6}Na^2\nabla^2 q_H-W^A(\mathbf{r})q_H, \tag{16}$$

and the initial conditions $q_C(\mathbf{r},0)=1$ and $q_H(\mathbf{r},0)=1$ [21]. Because the two ends of the copolymer are distinct, a second end-segment distribution function, $q_C^\dagger(\mathbf{r},s)$, is defined similarly to $q_C(\mathbf{r},s)$ except that the monomers are labeled with an index $t=1-s$, which is zero at the B end of the chain. Hence it satisfies Eq. (15) with $\partial/\partial s$ replaced by $-\partial/\partial s$, and the boundary condition $q_C^\dagger(\mathbf{r},1)=1$. In terms of the end-segment distribution functions, the monomer densities are given by

$$\phi^A(\mathbf{r})=\frac{n_C}{n_C+gn_H}\frac{V}{\mathcal{Q}^C}\int_0^f ds q_C(\mathbf{r},s)q_C^\dagger(\mathbf{r},s) +\frac{n_H}{n_C+gn_H}\frac{V}{\mathcal{Q}^H}\int_0^g ds q_H(\mathbf{r},s)q_H(\mathbf{r},g-s) \tag{17}$$

$$\phi^B(\mathbf{r})=1-\phi^A(\mathbf{r})=\frac{n_C}{n_C+gn_H}\frac{V}{\mathcal{Q}^C}\int_f^1 ds q_C(\mathbf{r},s)q_C^\dagger(\mathbf{r},s). \tag{18}$$

The diffusion Eqs. (15) and (16) above can be solved by expanding all spatially dependent functions in terms of orthonormal eigenfunctions $g_i(\mathbf{r})$ of the Laplacian operator, $\frac{1}{6}Na^2\nabla^2 g_i(\mathbf{r})=-\lambda_i d^{-2}g_i(\mathbf{r})$ [22]. The eigenfunctions are chosen to have the symmetry of the ordered phase considered. If the phase is periodic, the dimensionless parameter d is a measure of the repeat distance in units of the polymer radius of gyration.

For our calculations, we used up to 40 eigenfunctions, enough so that the calculated free energies and phase boundaries did not change measurably with additional functions. The length of the homopolymer was chosen to be equal to that of the copolymer ($g=1$), a choice that yields lamellar phases that can be swollen indefinitely [23]. The interaction parameter was always set to $\chi N=11$, rather close to the critical point in the pure copolymer system for which $\chi_c N\simeq 10.49$ when $f=1/2$ [24]. For larger values of the incompatibility the calculations become increasingly difficult due to stronger segregation effects.

III. RESULTS

A. Rupture

The mean-field solutions yield free energy densities $\mathcal{F}(\phi_H,d_L)$ for all different phases, from which the global phase diagram can be obtained. The parameter d_L is the repeat distance of the lamellar phase, which is an irrelevant variable if the phase considered is not structured vertically, and ϕ_H measures the average homopolymer (or solvent) volume fraction. To determine regions of phase coexistence, it is convenient to introduce the thermodynamic potential

$$\mathcal{T}(\mu,d_L)=\mathcal{F}(\phi_H,d_L)-\mu\phi_H, \tag{19}$$

where the chemical potential μ coupling to the homopolymer volume fraction is defined by

$$\mu=\frac{\partial\mathcal{F}}{\partial\phi_H}. \tag{20}$$

The concentrations in two phases coexisting at constant repeat distance d_L are obtained as a function of chemical potential, μ, and spacing d_L, from the two equations

$$\mu(\phi_H^{(1)})=\mu(\phi_H^{(2)}), \tag{21}$$

$$\mathcal{T}(\mu(\phi_H^{(1)}),d_L)=\mathcal{T}(\mu(\phi_H^{(2)}),d_L). \tag{22}$$

Our results for $f=0.49$, an architecture in which the lipid heads are slightly smaller than the tails, is shown in Fig. 1. There is a dilute, disordered phase, D, for large values of the homopolymer concentration ϕ_H, normal $H_{\rm I}$ and inverted $H_{\rm II}$ hexagonal phases, and a lamellar phase of bilayers, L. From the numerical calculations, it appears that the lamellar phase unbinds continuously to the disordered phase. If this be so, one expects the average volume fraction of the homopolymer to vary as

$$\phi_H \approx \phi_H^D + \frac{\delta}{d_L}(\phi_H^{Bl} - \phi_H^D), \tag{23}$$

where ϕ_H^D and ϕ_H^{Bl} are the volume fractions of homopolymer in the disordered phase produced at the unbinding transition and within the bilayer, respectively, and δ denotes the thickness of the bilayer. A plot of $1/d_L^*$, the value of the inverse separation in the system under zero stress and at equilibrium versus ϕ_H is shown in Fig. 2, and yields the expected linear relation. Vertical copolymer density profiles $\phi_C(z)$ for the system in equilibrium and under zero stress are shown in Fig. 3 for homopolymer densities of $\phi_H=0.1$ (short dashes), $\phi_H=0.5$ (long dashes), and $\phi_H=0.7$ (solid line). The profiles indeed demonstrate that the swelling of the lamellar phase leaves the bilayer structure unchanged (compare the central part of the lipid concentration profile for $\phi_H=0.5$ and 0.7); this means specifically that the bilayer thickness δ, under stress-free conditions, is independent of the bilayer separation for large separations.

We interpret the boundary between lamellar phase and the coexistence region with the disordered phase to denote the onset of rupture, because any further decrease in the spacing, due to a boundary condition or an external force, will induce disordered regions to appear in the lamellae at equilibrium. These disordered regions are laterally incorporated into the bilayers, leading to a fragmented state of the membrane in which the solvent layers on either side are topologically connected. At the boundary between lamellar phase and the coexistence region with the hexagonal phases any further increase of the spacing leads to the formation of hexagonal phase both laterally and, if d_L is allowed to relax locally, on top of the lamellae. The phase diagram in Fig. 1 corresponds to the experimental situation of a bilayer system between walls parallel to the lamellae, thereby fixing the mean repeat distance. By treating d_L as the parameter characterizing the strain in the lamellar system, we tacitly assume the number of bilayers between the plates to be constant. This also corresponds to the case of a single membrane between hard walls neglecting boundary effects, which is an acceptable approximation if the spacing is larger than the radius of gyration, i.e., $d_L>1$. If the number of bilayers between the plates is free to vary, one expects transitions between phases

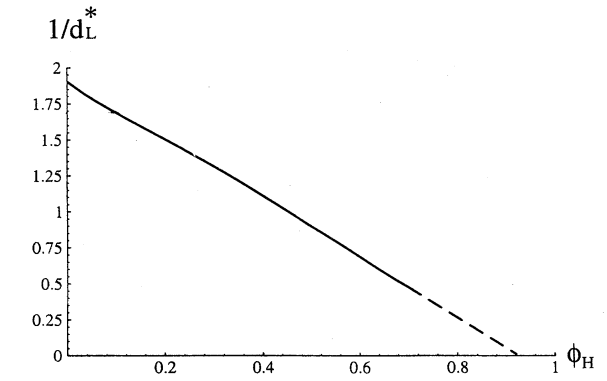

FIG. 2. Inverse repeat distance $1/d_L^*$ in the equilibrium system under zero stress as a function of solvent concentration ϕ_H. Linear extrapolation to $1/d_l^*=0$, shown by dashed line, gives the solvent concentration infinitely far from the bilayers.

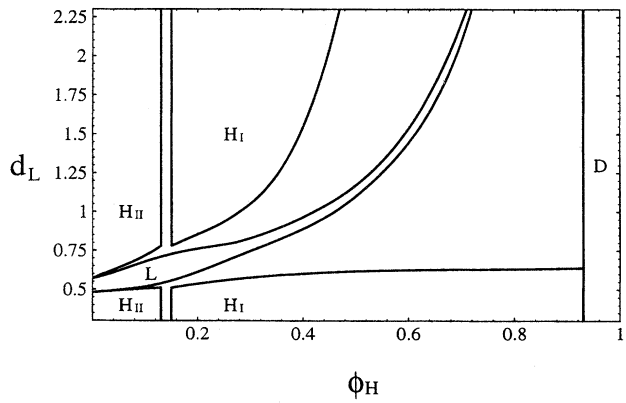

FIG. 1. Phase diagram for a nearly symmetric lipid (heads slightly less bulky than tails, $f=0.49$) as a function of solvent, or homopolymer concentration, ϕ_H and repeat distance d_L. There exists a lamellar phase (L), hexagonal and inverted hexagonal phases ($H_{\rm I}$ and $H_{\rm II}$), and a disordered state (D). Coexistence regions are not labeled. It appears that the lamellar phase can be swollen indefinitely, and thus reaches the disordered phase only for $d_L\to\infty$. The coexistence between the lamellar and disordered phases corresponds to a fragmentation, or rupture, of the bilayer upon compression.

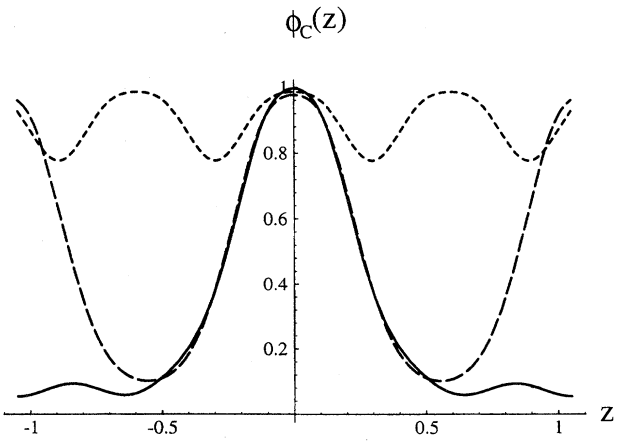

FIG. 3. Lipid, or copolymer, equilibrium concentration profiles $\phi_C(z)=1-\phi_H(z)$ as a function of the vertical coordinate for three different values of the average solvent concentration ϕ_H: $\phi_H=0.7$ and $d_L^*=2.3$ (short dashes), $\phi_H=0.5$ and $d_L^*=1.11$ (long dashes), $\phi_H=0.1$ and $d_L^*=0.6$ (solid line). For large dilutions, the bilayer structure, i.e., the core of the concentration profile, is rather insensitive to the separation, and the bilayer thickness is constant.

with different values of d_L [25].

The fractional change in area, $\alpha \equiv \delta A/A$, at the onset of rupture is plotted in Fig. 4. The lower curve corresponds to in-plane expansion, and the upper curve to in-plane compression. Both curves are essentially constant for relative separations larger than $d_L/\delta \approx 2$, so that these constant values would characterize isolated bilayers. This asymptotic value for area extension is about $\alpha \approx 0.02$, which compares quite well with experimental results on red blood cell membranes [13].

Other information that is of use to experiment can be extracted from the free energy density. Let us assume that the system is under a compressive stress σ, coupling to the repeat distance d_L, so that the work done in changing d_L by Δd_L is $A\sigma\Delta d_L$. For an incompressible system,

$$\sigma = d_L \frac{\partial \mathscr{F}}{\partial d_L}. \tag{24}$$

This derivative is only nonzero in the lamellar phase, of course. At coexistence with one of the other phases, a plate, such as in a surface force apparatus, would experience a reaction force $\bar{\sigma}$ proportional to the amount of the lamellar phase present, an amount given by the usual lever rule:

$$\bar{\sigma} = \sigma^{(L)} \frac{(\phi_H - \phi_H^{(2)})}{(\phi_H^{(L)} - \phi_H^{(2)})}. \tag{25}$$

Since the stress in the vertically unstructured phases is zero, there can be no force equilibrium between coexisting lamellar and unstructured phases; phase equilibrium is determined by free energy minimization alone. The relative volume fractions of the coexisting phases are determined by (21) and (22); the resulting d_L of the vertically unstructured phases will conform at no free energy cost to the external boundaries. Mechanical instability occurs when $\Delta\bar{\sigma}/\Delta d_L = 0$. A diagram showing the phase behavior as a function of $\bar{\sigma}$ and ϕ_H is presented in Fig. 5. Negative values of $\bar{\sigma}$ correspond to compression. When these values are of sufficient magnitude and the homopolymer concentration is small, the lamellar phase becomes mechanically unstable when coexistence with the inverted H_{II} hexagonal phase is reached. However, at larger homopolymer concentrations, when the lamellar phase reaches coexistence with the disordered phase (i.e., *ruptures*), the two-phase system remains mechanically stable as a whole. That is, an increase in the stress is needed to produce additional amounts of the disordered phase. Similarly, there is a small, mechanically stable region of coexistence with the normal hexagonal phase H_I. Under negative pressure, corresponding to positive $\bar{\sigma}$, there is no stable coexistence. Note that in the limit of extreme dilution, the lamellar phase is unstable to the smallest force exerted on the system of solvent and lipid. As noted above, these results would be applicable to experiments carried out on a lamellar phase of water and lipid in a surface force apparatus.

The results for an electroporation experiment are subtly different. Because water is such a good conductor, the pressure due to the electric field, σ_E, is not applied to the entire unit of water and lipid of thickness d_L, but almost solely to the lipid bilayer of thickness δ [15]. As a consequence, we cannot obtain σ_E directly from our calculated free energy

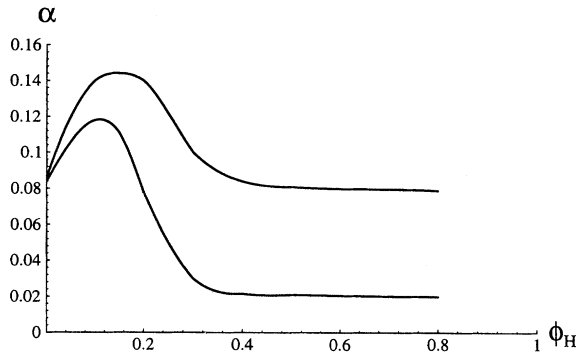

FIG. 4. Relative area change α at the onset of membrane rupture in the same system as in Fig. 1 upon area extension (or vertical compression, lower curve) and area compression (or vertical extension, upper curve).

density as it yields pressures, $d_L \partial\mathscr{F}/\partial d_L$, that would compress the entire repeat distance uniformly. However, we can find an equivalent pressure that, on acting through the displacement Δd_L, does the same work as σ_E acting through the displacement $\Delta\delta$;

$$\sigma_E = \frac{\Delta d_L}{\Delta \delta}\left(d_L \frac{\partial \mathscr{F}}{\partial d_L}\right). \tag{26}$$

We now use a result of our calculation that the bilayer thickness, defined as the distance between loci at which the copolymer concentration falls to 0.5, is linearly related to the repeat distance so that $\Delta d_L/\Delta\delta = d_L/\delta$. Therefore the electrostrictive force per unit area, σ_E, can be calculated from our free energy according to

$$\sigma_E = \frac{d_L^2}{\delta} \frac{\partial \mathscr{F}}{\partial d_L}. \tag{27}$$

We note that the product $\delta\sigma_E$ corresponds to the surface tension acting on the bilayer, and can be directly calculated from the free energy of the lamellar phase. The phase diagram in terms of $\delta\sigma_E$ and concentration ϕ_H is plotted in Fig.

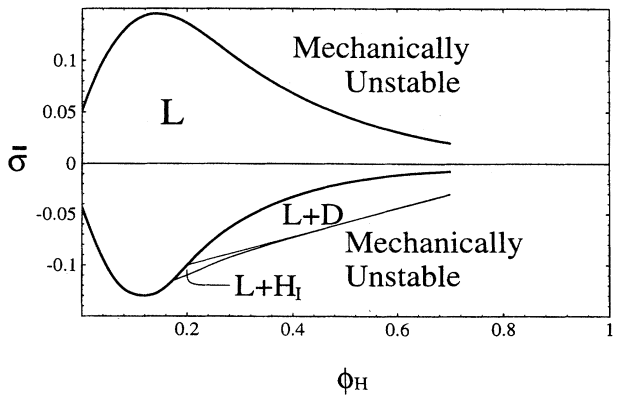

FIG. 5. Phase diagram for $f = 0.49$ as a function of the average vertical stress or pressure $\bar{\sigma}$.

6. Note that in distinction to Fig. 5 appropriate to a force apparatus, the value of $\delta\sigma_E$ asymptotes to a nonzero value in the limit of extreme dilution. Thus there is a threshold electric field that must be exceeded to produce rupture in a single membrane. This is in agreement with experiment [14,17]. Lastly we note that in the coexistence regions, we do not plot a value of $\delta\sigma_E$ weighted by the amount of lamellar phase in the system because the electrostriction does not act on the aqueous disordered phase, but only on the bilayer. This is in contrast to the surface force apparatus, which conveys a force from the entire plate to the lamellar phase, even though this phase may occupy only a fraction of the volume between plates.

Just as there is a difference between the two cases in which the entire system responds uniformly to an applied pressure, or only the bilayer resists this pressure, so there is a difference in the compressibility moduli that characterize this resistance. In the former case, we calculate the vertical compressibility modulus,

$$K_V \equiv d_L^2 \frac{\partial^2 \mathcal{F}(d_L)}{\partial d_L^2}, \tag{28}$$

while in the latter we consider

$$K_A \equiv d_L^3 \frac{\partial^2 \mathcal{F}(d_L)}{\partial d_L^2}, \tag{29}$$

which is denoted the area compressibility modulus. These moduli, evaluated for the system in equilibrium and under zero stress, are plotted in Fig. 7 as a function of homopolymer fraction. For large homopolymer concentrations, the vertical compressibility K_V (solid line) extrapolates to zero, whereas K_A (broken line) clearly approaches a finite value, which parallels the behavior of the corresponding stresses at the onset of rupture.

Finally, we comment on a fundamental difference between experiments in which a vertical pressure is applied to the membrane, and those in which a surface tension is applied to it. The former includes the two experimental situations we have considered, those involving a surface force apparatus (with fixed number of layers or only one layer), and electroporation experiments [17]. The latter encompasses experiments in which vesicles are deformed [13,14], or membranes on a frame are stretched. In these latter situations, the membrane mediates the surface tension, which is removed when the membrane fragments. Therefore rupture is always energetically favored, even for small strains and tensions, at least in the thermodynamic limit of membranes of infinite area. However, the activation energy for the rupture processes can be extremely high, leading to a long-lived metastable state, which makes the measurement of a threshold tension for rupture possible even in these situations. For finite systems, the line tension plays an important role in determining whether for a given stress the membrane will rupture or not [27]. Unlike these latter situations, our results apply to experiments in which the stress is imposed even in the ruptured or porated state.

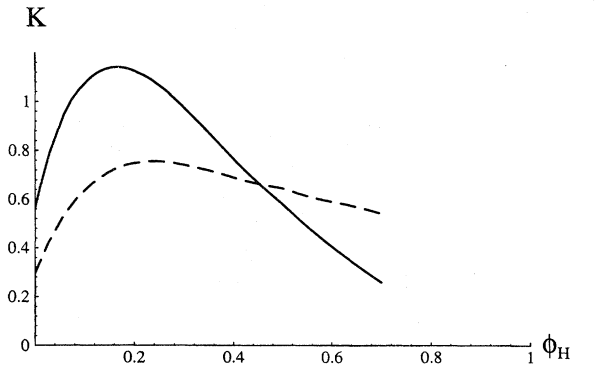

FIG. 7. Vertical compressibility modulus K_V, solid line, and area compressibility modulus K_A, broken line, as a function of solvent volume fraction.

B. Pore formation

In order to investigate the formation of pores, we consider a copolymer architecture which produces a stable catenoid lamellar phase. Such a phase can be considered to be a lamellar phase in which pores that pierce the bilayer con-

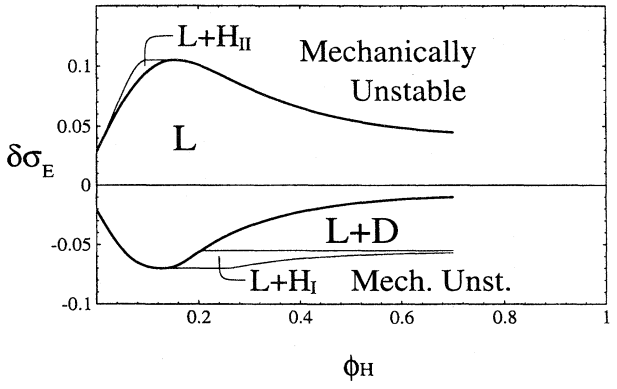

FIG. 6. Phase diagram for $f=0.49$ as a function of applied electroexpansive, ($\sigma_E>0$), or electrocompressive, ($\sigma_E<0$), force per unit area. The product $\delta\sigma_E$ corresponds to the surface tension, with δ being the bilayer thickness.

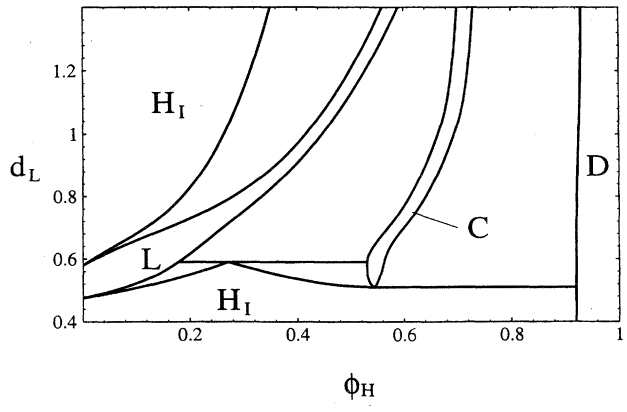

FIG. 8. Phase diagram for symmetric lipids ($f=0.5$) as a function of solvent concentration ϕ_H and repeat distance d_L. In addition to the phases in Fig. 1, there is a catenoid lamellar phase (C), which corresponds to an ordered array of pores.

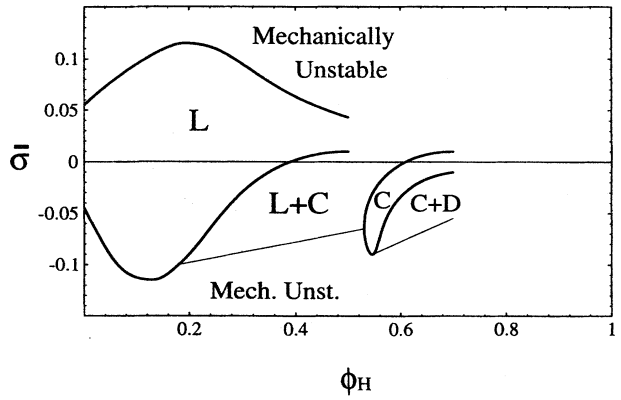

FIG. 9. Phase diagram for $f=0.5$ as a function of the average stress $\bar{\sigma}$ and homopolymer concentration.

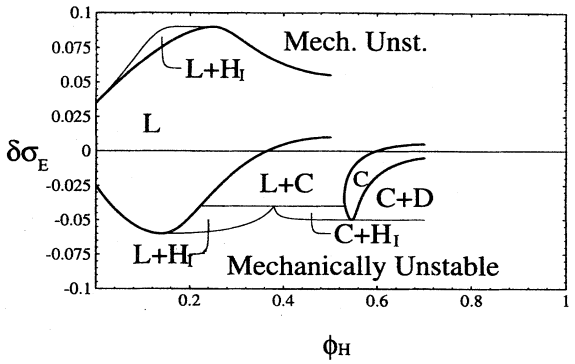

FIG. 10. Phase diagram for $f=0.5$ as a function of $\delta\sigma_E$ and homopolymer concentration.

dense into a hexagonal array. By this means we can examine the pore structure in such an array with the reasonable expectation that it does not differ greatly from the structure of an isolated pore. Pore structures have been considered in a number of phenomenological theories before [28,29]. We want to determine, in particular, whether the head groups in the core rearrange themselves significantly to shield the hydrophobic portions, producing a "hydrophilic core," or do

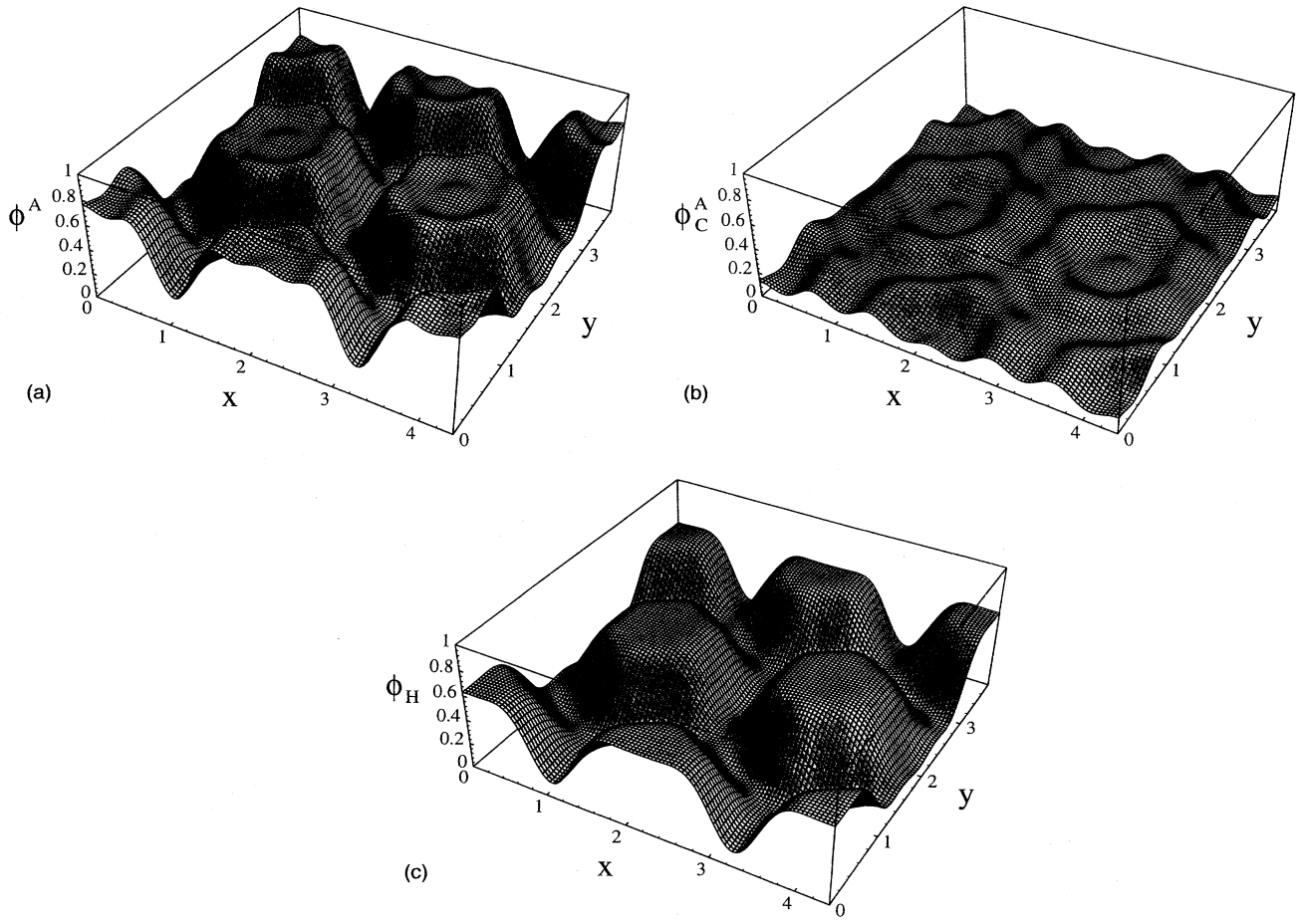

FIG. 11. (a) Total A-monomer concentration, (b) the copolymer A monomer (or lipid heads), (c) the solvent concentration in the center of a bilayer for $d_L=1.03$ in the catenoid lamellar phase.

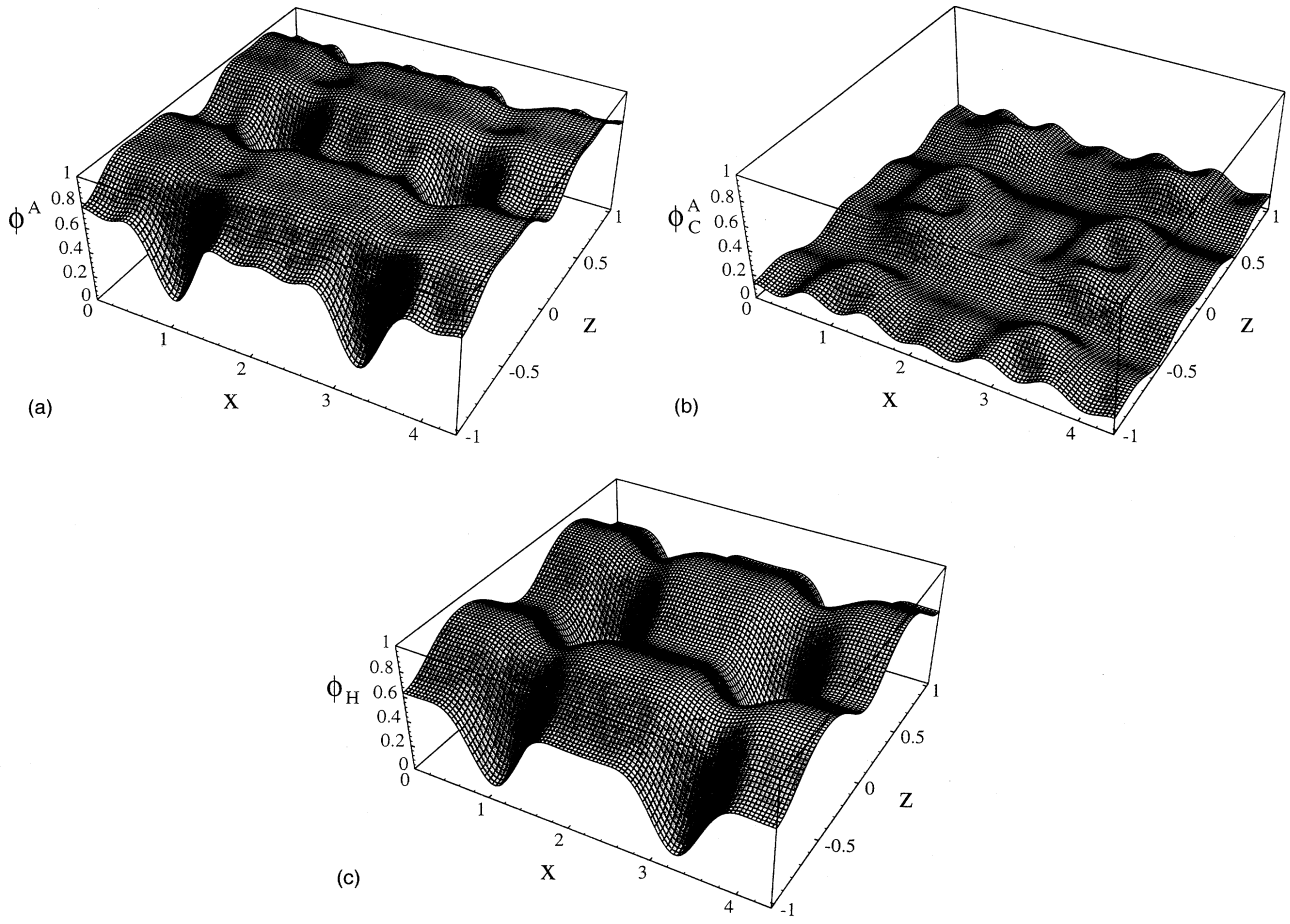

FIG. 12. Monomer concentrations of component A in the vertical plane for $y=0$. (a) Total A-monomer concentration, (b) the copolymer A-monomer (or lipid heads), (c) the solvent concentration.

not significantly rearrange, leaving a "hydrophobic" core. We choose for this purpose the symmetric copolymer, $f=0.5$.

The phase diagram is shown in Fig. 8 as a function of the spacing d_L. It now contains a catenoid lamellar phase (C), and only normal hexagonal phases. The phase diagram is shown in terms of the average stress, and for uniform d_L appropriate to a force apparatus, in Fig. 9. A large coexistence region between the lamellar phase and the catenoidal phase appears at moderate compressive stress. Figure 10 shows the phase diagram in terms of the electrostrictive stress, appropriate to electroporation. Here, the repeat distances of coexisting catenoidal and lamellar phases are in general different [26]. As far as extrapolation is possible, the phase boundaries seem to approach finite values as the separation between the bilayers grows without limit, again indicating a threshold electric field for rupture or pore formation.

Concentration profiles in the catenoid lamellar phase are shown in the next several figures. Figure 11 shows several profiles, all at the point in the phase diagram at which $d_L=1.03$ and the lamellar and catenoid lamellar phases coexist. The concentrations are calculated in the $z=0$ plane parallel to, and at the midpoint of, the bilayer. The total monomer-A concentration, $\phi^A=\phi_C^A+\phi_H$, is shown in Fig. 11(a), the lipid head concentration ϕ_C^A in (b), and the solvent concentration ϕ_H in (c). Figure 12 shows the same three concentrations displayed in the $y=0$ plane perpendicular to the plane of the bilayer.

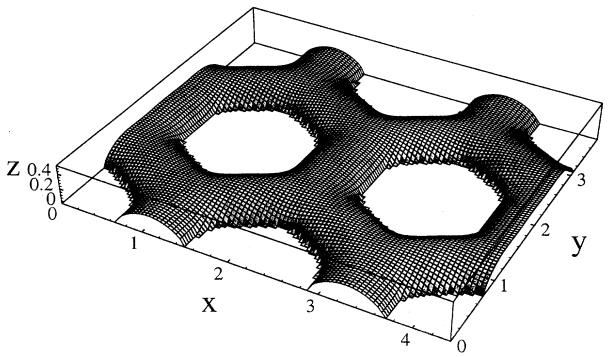

FIG. 13. Bilayer surface in the catenoidal phase for $d_L=1.03$. All distances are measured in units of the polymer radius of gyration.

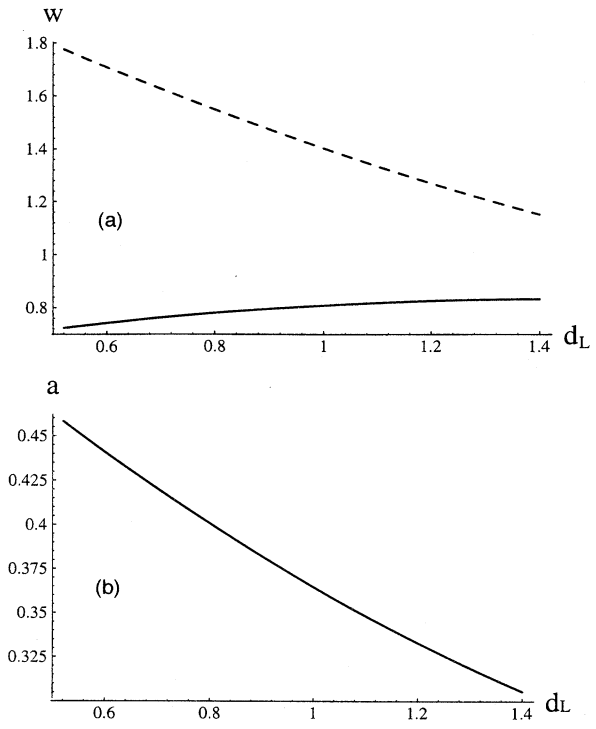

FIG. 14. (a) Width of the pores (broken lines) and width of the membrane bridges in the symmetry plane of the bilayers and for $y=0$. The widths are measured in units of the polymer radius of gyration, as is d_L. (b) fractional area of the pores for $d_L=1.03$.

The membrane surface, defined as the locus of points at which the copolymer concentration has decreased to $\phi_C=1/2$, is shown in Fig. 13. The diameter of the holes and the width of the membrane bridge defined along the axis $z=0$ and $y=0$ are plotted in Fig. 14(a). The width of the membrane bridge stays rather constant and the diameter of individual pores decreases as d_L, and the solvent concentration ϕ_H, increase. The fractional area of the holes are plotted as a function of the repeat distance in Fig. 14(b). As the separation between membranes increases, the pores become smaller.

Since the bilayer thicknesses of the coexisting lamellar and catenoidal phases are very similar, it is likely that the line tension between these two phases is small. If so, single pores that dissolve in the lamellar phase would undergo thermally activated diffusion. A measure of how easily pores can move is provided by their compressibility modulus in the plane,

$$K_H=d_H^2\frac{\partial^2\mathcal{F}(d_L,d_H)}{\partial^2 d_H}, \tag{30}$$

where d_H is the lattice constant of the hexagonal array of pores. This quantity, normalized by the vertical compressibility K_V in the lamellar phase at coexistence, is plotted in Fig. 15 as the broken line. The vertical compressibility modulus in the catenoid lamellar phase, normalized by the same

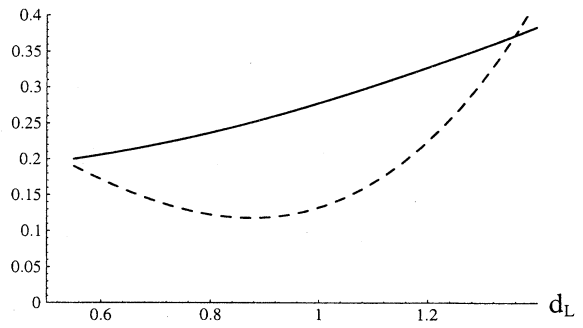

FIG. 15. In-plane compressibility due to displacement of pores normalized by the vertical compressibility of the lamellar phase, $K_H(C)/K_V(L)$, broken line, and vertical compressibility of the catenoid phase normalized by the vertical compressibility of the lamellar phase, $K_L(C)/K_V(L)$. Results are at coexistence of catenoid and lamellar phase, and plotted as a function of the repeat distance d_L.

modulus in the lamellar phase, is shown as a solid line. Both ratios are smaller than unity, which shows that the catenoidal phase is much softer than the coexisting lamellar phase.

To determine whether the pores are "hydrophilic" or "hydrophobic," we consider the quantity $2(\phi_C^A-\phi_C^B)$, which is twice the difference between the volume fraction of head groups A and tail groups B in the copolymer. We evaluate it on the surface of the membrane as a function of position, and refer to it as the hydrophilicity. Because $(\phi_C^A+\phi_C^B)=1/2$ on the surface by definition, the hydrophilicity is simply $(\phi_C^A-\phi_C^B)/(\phi_C^A+\phi_C^B)$. Figure 16(a) shows a cross section in the $y=0$ plane of the membrane surface of Fig. 13. The value of the hydrophilicity on this surface is shown in Fig. 16(c). We see that as x increases and we descend into the pore, the hydrophilicity decreases and becomes negative, so that there are more tails B than heads A exposed to the A homopolymer. Thus the pores in this cross section are slightly "hydrophobic." A similar cross section in the $x=0$ plane with its associated values of hydrophilicity are shown in Figs. 16(b) and 16(d). In this direction, the hydrophilicity falls only to zero. On average, therefore, the pores are weakly hydrophobic.

The self-consistent mean-field theory also yields *metastable* solutions corresponding to saddle points in the free energy. These saddle-point structures provide insight into the energetics of transformations between different phases. In Fig. 17 we show the surface of the metastable solution, which connects the lamellar and the catenoidal phase for $d_L=1.03$. This structure is a bilayer with a very weak surface modulation. We have expanded the vertical scale in the figure to make the structure more easily visible. As can be surmised from the weakness of the modulation, the free energy is only slightly higher than the lamellar phase itself. It follows that the activation barrier for the formation of the catenoidal phase is actually very small. Thus one expects that the formation of such a pore structure would proceed via a moderate surface modulation of the bilayers, rather than by means of the formation of hydrophobic microholes [28].

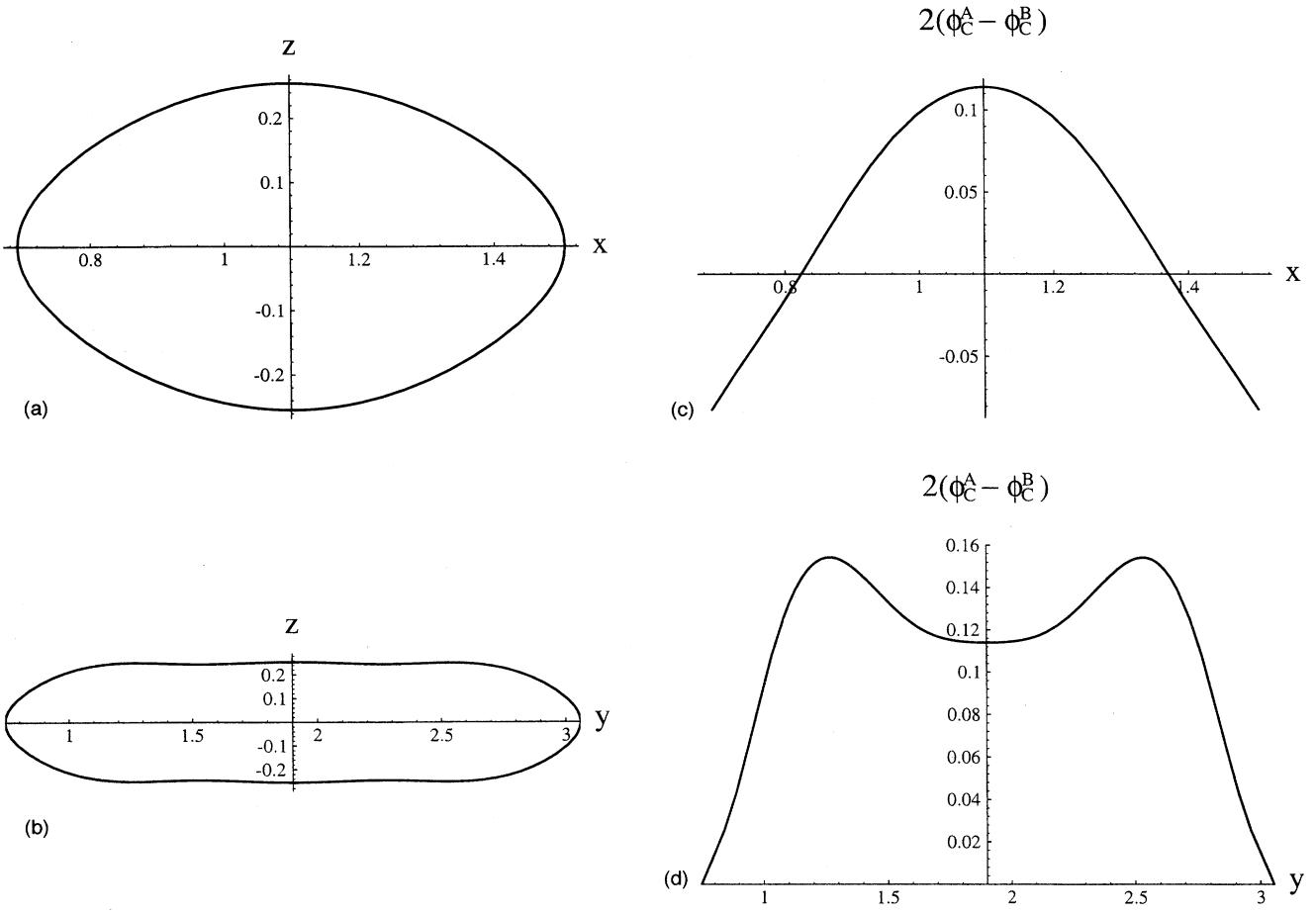

FIG. 16. Two-dimensional projections of the bilayer surface for (a) $y=0$ and for (b) $x=0$. Hydrophilicity, $2(\phi_C^A - \phi_C^B)$, evaluated at the bilayer surface for (c) $y=0$ and for (d) $x=0$. The pore centers are slightly hydrophobic.

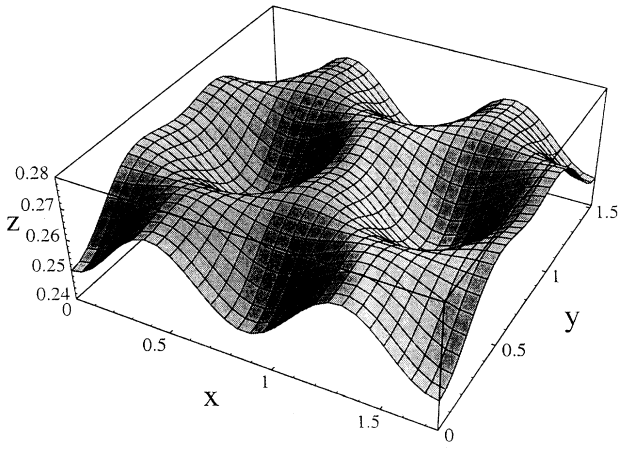

FIG. 17. Bilayer surface of the metastable solution at $d_L=1.03$, corresponding to a saddle point between lamellar and catenoidal solutions in the free energy landscape.

IV. SUMMARY

A polymeric model was used to investigate the behavior of bilayers under the action of mechanical stress. It was solved using a numerical implementation of the self-consistent field theory. In the absence of stress, and for suitably chosen head to tail volume ratios, the model yields stacks of bilayers that are separated by layers of solvent. Due to the complexity of the numerical calculations involved, we could consider the system only in relatively weak segregation between the lipids and the surrounding solvent. Nevertheless, many of the salient properties of real membranes already appear in our calculations.

We find that under an external force the repeat distance, and concomitantly, the bilayer thickness, changes until the bilayer coexists thermodynamically with either the disordered phase, or the catenoid lamellar phase. We interpret the first as the onset of rupture, and the second as the formation of pores. Both phenomena occur in equilibrium, and are therefore reversible, in accord with electroporation experiments. Which process occurs depends on the architecture of the basic membrane component.

The relative area increase at the onset of rupture is approximately 2% for bilayers that are far apart, a value that compares favorably with experiment. We analyze the struc-

ture of the pores, and find them to be slightly hydrophobic.

We also obtain metastable structures corresponding to saddle points in the free energy for the formation of pores. These structures are slightly modulated versions of the unperturbed bilayers with only a small increase in the free energy.

Pores have also been considered theoretically in the framework of phenomenological elasticity theory [6,28,29]. Using our results, we can confirm many of the underlying assumptions of those theories regarding the structure of the pores. Very recently, the formation of holes in two-dimensional tethered polymer networks was observed including the effects of fluctuations [30]. Analogously, one might expect thermally excited pores even in the lamellar phase of our polymeric model.

ACKNOWLEDGMENTS

One of us (M.S.) is grateful to Michael Wortis for seminal conversations, and we both thank him and Frank Jülicher for useful discussions. This work was supported by the National Science Foundation under Award No. DMR-9220733. R.R.N. acknowledges receipt of a NATO science stipend administered by the DAAD.

[1] *Statistical Mechanics of Membranes and Surfaces*, edited by D. Nelson, T. Piran, and S. Weinberg (World Scientific, Singapore, 1989).

[2] M. Bloom, E. Evans, and O.G. Mouritsen, Quart. Rev. Biophys. **24**, 293 (1991).

[3] S.A. Safran, *Statistical Thermodynamics of Surfaces, Interfaces, and Membranes* (Addison-Wesley, Reading, 1994).

[4] *Micelles, Membranes, Microemulsions, and Monolayers*, edited by W.M. Gelbart, A. Ben-Shaul, and D. Roux (Springer, New York, 1994); *Handbook for Membranes*, edited by R. Lipowsky and E. Sackmann (Springer, New York, 1995).

[5] G. Gompper and M. Schick, in *Phase Transitions and Critical Phenomena*, edited by C. Domb and J.L. Lebowitz (Academic, London, 1994), Vol. 16.

[6] A good review with an extensive list of references is given in D.S. Dimitrov and R.K. Jain, Biochim. Biophys. Acta **779**, 437 (1984).

[7] R.P. Rand and A.C. Burton, Biophys. J. **4**, 115 (1964).

[8] R.P. Rand, Biophys. J. **4**, 303 (1964).

[9] E.A. Evans, Biophys. J. **16**, 597 (1976)

[10] E.A. Evans and D. Needham, J. Phys. Chem. **91**, 4219 (1987), and references therein.

[11] E.A. Evans and R.M. Hochmuth, Biophys. J. **16**, 13 (1976).

[12] R.E. Waugh, Biophys. J. **39**, 273 (1982).

[13] E. Evans, R. Waugh, and L. Melnick, Biophys. **16**, 585 (1976); E. Evans and R. Waugh, *ibid.* **20**, 307 (1977); R. Kwok and E. Evans, *ibid.* **35**, 637 (1981).

[14] D. Needham and R.M. Hochmuth, Biophys. J. **55**, 1001 (1989).

[15] J.M. Crowley, Biophys. J. **13**, 711 (1973); U.G. Zimmermann, A. Pilwat, A. Pequeux, and R. Gilles, J. Membr. Biol. **54**, 103 (1980).

[16] U. Zimmermann, Biochim. Biophys. Acta **694**, 227 (1982).

[17] *Guide to Electroporation and Electrofusion*, edited by D.C. Chang, B.M. Chassy, J.A. Saunders, and A.E. Sowers (Academic, San Diego, 1992).

[18] S. Marčelja, Biochem. Biophys. Acta **367**, 165 (1974); J.F. Nagle, J. Chem. Phys. **58**, 252 (1973); D. Marsh, J. Membrane Biol. **18**, 145 (1974); H.L. Scott, J. Theor. Biol. **46**, 241 (1974); I. Bivas and A. Derzhanski, Mol. Cryst. Liq. Cryst. **74**, 171 (1981), and references therein.

[19] I. Szleifer, D. Kramer, A. Ben-Shaul, D. Roux, and W.M. Gelbart, Phys. Rev. Lett. **60**, 1966 (1988).

[20] Y. Suezaki, J. Theor. Biol. **71**, 279 (1978); J. Colloid. Interface Sci. **73**, 529 (1980).

[21] E. Helfand, J. Chem. Phys. **62**, 999 (1975).

[22] M.W. Matsen and M. Schick, Phys. Rev. Lett. **72**, 2660 (1994); Macromolecules **27**, 6761 (1994).

[23] M. Matsen, Phys. Rev. Lett. **74**, 4225 (1995).

[24] L. Leibler, Macromolecules **13**, 1602 (1980).

[25] M.S. Turner, Phys. Rev. Lett. **69**, 1788 (1992).

[26] The coexisting catenoidal and lamellar phases in the ensemble of constant electrostrictive stress are obtained from minimizing the thermodynamic potential $\mathcal{G}(\mu,\delta\sigma_E)=\mathcal{F}(\phi_H,d_L)-\mu\phi_H+\delta\sigma_E/d_L$, which is obtained by Legendre transformation. Note that $\partial\mathcal{F}/\partial(-1/d_L)=d_L^2\partial\mathcal{F}/\partial d_L$ is, from Eq. (27), equal to $\delta\sigma_E$.

[27] D.V. Zhelev and D. Needham, Biochim. Biophys. Acta **1147**, 89 (1993).

[28] R.W. Glaser, S.L. Leikin, L.V. Chernomordik, V.F. Pastushenko, and A.I. Sokirko, Biochim. Biophys. Acta **940**, 275 (1988).

[29] S.A. Freeman, M.A. Wang, and J.C. Weaver, Biophys. J. **67**, 42 (1994).

[30] J.C. Shillcock and D.H. Boal (unpublished).

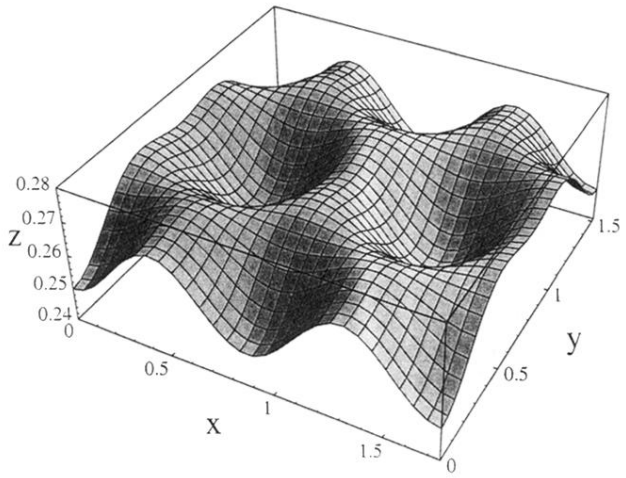

FIG. 17. Bilayer surface of the metastable solution at $d_L = 1.03$, corresponding to a saddle point between lamellar and catenoidal solutions in the free energy landscape.